SUPERMASSIVE BLACK HOLE AND HOST BULGE AFFAIRS
II. THE EARLY AND LATE SEQUENCE IN THE $M_{\rm BH} - M_{*,\rm SPH}$ DIAGRAM

Giulia A. D. Savorgnan and Alister W. Graham
Centre for Astrophysics and Supercomputing, Swinburne University of Technology, Hawthorn, Victoria 3122, Australia.

Alessandro Marconi
Dipartimento di Fisica e Astronomia, Universitá di Firenze, via G. Sansone 1, I-50019 Sesto Fiorentino, Firenze, Italy.

and

Eleonora Sani
European Southern Observatory, Alonso de Cordova, Vitacura 3107, Santiago, Chile.
Draft version May 29, 2015

ABSTRACT

In our first paper, we performed a detailed (i.e. bulge, disks, bars, spiral arms, rings, halo, nucleus, depleted core, etc.) decomposition of 66 galaxies, with directly measured black hole masses, that had been imaged at 3.6 μm with *Spitzer*. Our sample is the largest to date and, for the first time, the decompositions were checked for consistency with the galaxy kinematics. We present correlations between the black hole mass, $M_{\rm BH}$, and the host spheroid (and galaxy) luminosity, $L_{\rm sph}$ (and $L_{\rm gal}$), and also stellar mass, $M_{*,\rm sph}$. Most previous studies have used galaxy samples that were overwhelmingly dominated by high-mass, early-type galaxies. Instead, our sample includes 17 spiral galaxies, half of which have $M_{\rm BH} < 10^7$ M$_\odot$, and allows us to better investigate the poorly studied low-mass end of the $M_{\rm BH} - M_{*,\rm sph}$ correlation. The bulges of early-type (E + S0) galaxies follow $M_{\rm BH} \propto M_{*,\rm sph}^{1.04\pm0.10}$, consistent with a dry-merging formation scenario, and define a tight *early-type sequence* with intrinsic scatter $\epsilon_{(Y|X)} = 0.43 \pm 0.06$ dex. At the low-mass end, the bulges of late-type (Sp) galaxies define a much steeper *late-type sequence*, with $M_{\rm BH} \propto M_{*,\rm sph}^{2-3}$, indicating that gas-rich processes feed the black hole more efficiently than the host bulge as they coevolve. We additionally report that: i) Sérsic galaxies follow $M_{\rm BH} \propto M_{*,\rm sph}^{1.48\pm0.20}$, a less steep sequence than previously reported; ii) bulges with Sérsic index $n_{\rm sph} < 2$, argued by some to be pseudo-bulges, are not offset to lower $M_{\rm BH}$ from the correlation defined by bulges with $n_{\rm sph} > 2$; and iii) $L_{\rm sph}$ and $L_{\rm gal}$ correlate equally well with $M_{\rm BH}$, in terms of intrinsic scatter, only for early-type galaxies; once reasonable numbers of spiral galaxies are included, the correlation with $L_{\rm sph}$ is better than that with $L_{\rm gal}$.

Subject headings: galaxies: bulges; galaxies: elliptical and lenticular, cD; galaxies: evolution; galaxies: structure; black hole physics

1. INTRODUCTION

A quarter of a century ago, Dressler (1989) foresaw a "rough scaling of black hole mass with the mass of the spheroidal component" of galaxies, as suggested by the sequence of five galaxies (M87, M104, M31, M32 and the Milky Way). Yee (1992) then announced a linear relation between what was effectively black hole mass and galaxy mass for high-luminosity, bulge-dominated early-type galaxies radiating near the Eddington limit. This "rough scaling" was a premature version of the early correlations between black hole mass, $M_{\rm BH}$, and host spheroid luminosity, $L_{\rm sph}$, and also host spheroid mass, $M_{\rm sph}$ (Kormendy & Richstone 1995; Magorrian et al. 1998; Marconi & Hunt 2003; Häring & Rix 2004). These initial studies were dominated by high-mass, early-type galaxies, for which they too reported a quasi-linear $M_{\rm BH} - M_{\rm sph}$ relation. Subsequent studies of the $M_{\rm BH} - L_{\rm sph}$ and $M_{\rm BH} - M_{\rm sph}$ diagrams (Ferrarese & Ford 2005; Lauer et al. 2007a; Graham 2007; Gültekin et al. 2009; Sani et al. 2011; Beifiori et al. 2012; Erwin & Gadotti 2012;

Vika et al. 2012; van den Bosch et al. 2012; McConnell & Ma 2013; Kormendy & Ho 2013) continued to use galaxy samples dominated by high-mass, early-type systems with $M_{\rm BH} \gtrsim 0.5 \times 10^8$ M$_\odot$, and they too recovered a near-linear relation. However, the consensus about a linear $M_{\rm BH} - M_{\rm sph}$ correlation was not unanimous. Some studies had reported a slope steeper than one, or noticed that the low-mass spheroids were offset to the right of (or below) the relation traced by the high-mass spheroids (Laor 1998; Wandel 1999; Laor 2001; Ryan et al. 2007). Graham (2012), Graham & Scott (2013) and Scott et al. (2013) found two distinct trends in the $M_{\rm BH} - L_{\rm sph}$ and $M_{\rm BH} - M_{\rm sph}$ diagrams: a linear and a super-quadratic correlation at the high- and low-mass end, respectively[1]. Recently, Läsker et al. (2014a,b) derived 2.2 μm bulge luminosities for 35 galaxies (among which only 4 were classified as spiral galaxies), and reported a slope below unity for their $M_{\rm BH} - L_{\rm sph}$ relation. They also claimed that the black hole mass correlates equally well with the

gsavorgn@astro.swin.edu.au

---

[1] Readers interested in an extensive review about the early discovery and successive improvements of these correlations should consult Graham (2015b).

total galaxy luminosity as it does with the bulge luminosity.

The $M_{\rm BH} - L_{\rm sph}$ relation for early-type (elliptical + lenticular) galaxies can be predicted by combining two other correlations that involve the bulge stellar velocity dispersion, σ. One of these is the $M_{\rm BH} - \sigma$ relation (Ferrarese & Merritt 2000; Gebhardt et al. 2000), which can be described with a single power-law ($M_{\rm BH} \propto \sigma^{5-6}$) over a wide range in velocity dispersion ($70 - 350$ km s^{-1}, e.g. Graham et al. 2011; McConnell et al. 2011; Graham & Scott 2013). The other is the $L_{\rm sph} - \sigma$ relation, which has long been known to be a "double power-law", with $L_{\rm sph} \propto \sigma^{5-6}$ at the luminous end[2] (Schechter 1980; Malumuth & Kirshner 1981; von der Linden et al. 2007; Lauer et al. 2007b; Liu et al. 2008) and $L_{\rm sph} \propto \sigma^2$ at intermediate and faint luminosities (Davies et al. 1983; Held et al. 1992; Matković & Guzmán 2005; de Rijcke et al. 2005; Balcells et al. 2007; Chilingarian et al. 2008; Forbes et al. 2008; Cody et al. 2009; Tortora et al. 2009; Kourkchi et al. 2012). The change in slope of the $L_{\rm sph} - \sigma$ relation occurs at $M_B \approx -20.5$ mag, corresponding to $\sigma \approx 200$ km s^{-1}. The $M_{\rm BH} - L_{\rm sph}$ relation should therefore be better described by a "broken", rather than a single power-law: with $M_{\rm BH} \propto L_{\rm sph}^{2.5}$ at the low-luminosity end, and $M_{\rm BH} \propto L_{\rm sph}^{1}$ at the high-luminosity end. Due to the scatter in the $M_{\rm BH} - L_{\rm sph}$ (or $M_{\rm BH} - M_{\rm sph}$) diagram, studies that have not sufficiently probed below $M_{\rm BH} \approx 10^7$ M$_\odot$ can easily miss the change in slope occuring at $M_{\rm BH} \approx 10^{(8\pm1)}$ M$_\odot$, and erroneously recover a single log-linear relation.

When Graham (2012) pointed out this overlooked inconsistency between these linear and bent relations, he identified two different populations of galaxies, namely the core-Sérsic spheroids (Graham et al. 2003; Trujillo et al. 2004) and the Sérsic spheroids[3], and attributed the change in slope (from super-quadratic to linear) to their different formation mechanisms. In this scenario, core-Sérsic spheroids are built in dry merger events where the black hole and the bulge grow at the same pace, increasing their mass in lock steps ($M_{\rm BH} \propto L_{\rm sph}^{1}$), whereas Sérsic spheroids originate from gas-rich processes in which the mass of the black hole increases more rapidly than the mass of its host spheroid ($M_{\rm BH} \propto L_{\rm sph}^{2.5}$).

Graham & Scott (2013, hereafter GS13) and Scott et al. (2013) presented separate power-law linear regressions for the Sérsic and core-Sérsic spheroids in the $M_{\rm BH} - L_{\rm sph}$ and $M_{\rm BH} - M_{*,\rm sph}$ (spheroid stellar mass) diagrams, probing down to $M_{\rm BH} \approx 10^6$ M$_\odot$. To obtain their dust-corrected *bulge* magnitudes, they did not perform bulge/disc decompositions, but converted the $B-$band and K_S-band observed, total *galaxy* magnitudes into bulge magnitudes using a mean statistical bulge-to-total ratio based on each object's morphological type and disc inclination[4]. These mean statistical bulge-to-total ratios

were obtained from the results of two-component (Sérsic-bulge/exponential-disk) decompositions in the literature. Here we investigate substructure in the $M_{\rm BH} - L_{\rm sph}$ and $M_{\rm BH} - M_{*,\rm sph}$ diagrams using state-of-the-art galaxy decompositions (Savorgnan & Graham 2015, hereafter *Paper I*) for galaxies with directly measured black hole masses. Our galaxies are large and nearby, which allows us to perform accurate multicomponent decompositions (instead of simple bulge/disk decompositions). Our decompositions were performed on 3.6 μm *Spitzer* satellite imagery, which is an excellent proxy for the stellar mass, superior to the $K-$band (Sheth et al. 2010, and references therein). Nine of our galaxies have $M_{\rm BH} \lesssim 10^7$ M$_\odot$, which allows us to better constrain the slope of the correlation at the low-mass end. Furthermore, our galaxy sample includes 17 spiral galaxies, representing a notable improvement over past studies dominated by early-type galaxies. In a forthcoming paper, we will explore the relation between the black hole mass and the bulge dynamical mass, $M_{\rm dyn,sph} \propto R_{\rm e}\sigma^2$, and address the issue of a black hole fundamental plane.

2. DATA

Our galaxy sample (see Table 1) consists of 66 objects for which a dynamical measurement of the black hole mass had been tabulated in the literature (by GS13 or Rusli et al. 2013) at the time that we started this project, and for which we were able to obtain useful spheroid parameters from 3.6 μm *Spitzer* satellite imagery.

Spheroid magnitudes were derived from our state-of-the-art galaxy decompositions, which take into account bulge, disks, spiral arms, bars, rings, halo, extended or unresolved nuclear source and partially depleted core. Kinematical information (Emsellem et al. 2011; Scott et al. 2014; Arnold et al. 2014) was used to confirm the presence of rotationally supported disk components in most early-type (elliptical + lenticular) galaxies, and to identify their extent (intermediate-scale disks that are fully embedded in the bulge, or large-scale disks that encase the bulge and dominate the light at large radii). *Paper I* presents the dataset used here, including details about the data reduction process and the galaxy modelling technique that we developed. It also discusses how we estimated the uncertainties[5] on the bulge magnitudes, and presents the individual 66 galaxy decompositions, along with a comparison and discussion of past decompositions.

Bulge luminosities[6] (Table 1) from *Paper I* were con-

---

[2] Recent work has the $M_{\rm BH} - \sigma$ correlation as steep as $M_{\rm BH} \propto \sigma^{6.5}$ (Savorgnan & Graham 2015), and the high-luminosity end of the $L_{\rm sph} - \sigma$ correlation as steep as $L_{\rm sph} \propto \sigma^8$ (Montero-Dorta et al. 2015).

[3] Core-Sérsic spheroids have partially depleted cores relative to their outer Sérsic light profile, whereas Sérsic spheroids have no central deficit of stars.

[4] While this resulted in individual bulge magnitudes not being exactly correct, their large sample size allowed them to obtain a

reasonable $M_{\rm BH} - L_{\rm sph}$ relation for the ensemble.

[5] By comparing, for each of our galaxies, the measurements of the bulge magnitude obtained by different authors with that obtained by us, we estimated the uncertainties on the bulge magnitudes, in effect taking into account systematic errors. Systematic errors include incorrect sky subtraction, inaccurate masking of contaminating sources, imprecise description of the PSF, erroneous choice of model components (for example, when failing to identify a galaxy subcomponent and thus omitting it in the model, or when describing a galaxy sub-component with an inadequate function), the radial extent of the surface brightness profile and one's sampling of this. Most of these factors are not included in popular 2D fitting codes which report only the random errors associated with their fitted parameters. In fact, when performing multi-component decomposition of high signal-to-noise images of nearby – therefore well spatially resolved – galaxies, errors are dominated by systematics rather than Poisson noise.

[6] Following Sani et al. (2011), absolute luminosities were calculated assuming a 3.6 μm solar absolute magnitude of 3.25 mag.

verted into stellar masses using a constant 3.6 μm mass-to-light ratio, $\Gamma_{3.6} = 0.6$ (Meidt et al. 2014). We additionally explored a more sophisticated way to compute mass-to-light ratios, using the color-$\Gamma_{3.6}$ relation published by Meidt et al. (2014, their equation 4), which allows one to estimate $\Gamma_{3.6}$ of a galaxy from its $[3.6]-[4.5]$ color. Individual $[3.6]-[4.5]$ colors[7] were taken from Peletier et al. (2012, column 8 of their Table 1) when available for our galaxies, or were estimated from the bulge stellar velocity dispersion, σ, using the color-σ relation presented by Peletier et al. (2012, their Figure 6). We found that the range in $[3.6]-[4.5]$ color is small (0.06 mag), and thus the range in $\Gamma_{3.6}$ is also small (0.04). After checking that using a single $\Gamma_{3.6} = 0.6$, independent of $[3.6]-[4.5]$ color, does not significantly affect the results of our analysis, we decided to use individual, color-dependent mass-to-light ratios.

For each galaxy, the total luminosity (or galaxy luminosity, $L_{\rm gal}$) is the sum of the luminosities of all its sub-components. Due to the complexity of their modelling, four galaxies (see Table 1, column 7) had their galaxy luminosities underestimated[8], which are given here as lower limits. Following GS13, we assumed a fixed uncertainty (0.25 mag) for the absolute galaxy magnitude $MAG_{\rm gal}$.

The morphological classification (E = elliptical; E/S0 = elliptical/lenticular; S0 = lenticular; S0/Sp = lenticular/spiral; Sp = spiral; and "merger") follows from the galaxy models presented in *Paper I*. Throughout this paper we will refer to early-type galaxies (E+S0) and late-type galaxies (Sp). Two galaxies classified as E/S0 are obviously included in the early-type bin, whereas two galaxies classified as S0/Sp and another two classified as mergers are included in neither the early- nor the late-type bin.

The Sérsic/core-Sérsic classification presented in this work comes from the compilation of Savorgnan & Graham (2015), who identified partially depleted cores according to the same criteria used by GS13. When no high-resolution image analysis was available from the literature, they inferred the presence of a partially depleted core based on the stellar velocity dispersion: a spheroid is classified as core-Sérsic if $\sigma > 270$ km s^{-1}, or as Sérsic if $\sigma < 166$ km s^{-1}. All of the galaxies with velocity dispersions between these two limits had high-resolution images available.

3. ANALYSIS

We performed a linear regression analysis of the $M_{\rm BH}-L_{\rm gal}$ (see Table 2), $M_{\rm BH}-L_{\rm sph}$ (see Table 3) and $M_{\rm BH}-M_{*,\rm sph}$ (see Table 4) data, using the BCES code from Akritas & Bershady (1996). We also repeated the analysis using both the FITEXY routine (Press et al. 1992), as modified by Tremaine et al. (2002), and the Bayesian estimator linmix_err (Kelly 2007). All of these three linear regression routines account for the intrinsic scatter, but only the last two allow one to quantify it. We report linear regressions, both symmetrical and non-symmetrical, for Sérsic/core-Sérsic and for early/late-type galaxies. Symmetrical regressions are meant to be

compared with theoretical expectations, whereas non-symmetrical forward ($M_{\rm BH}|X$) regressions – which minimize the scatter in the $\log(M_{\rm BH})$ direction – are best used to predict black hole masses.

4. RESULTS AND DISCUSSION

4.1. *Black hole mass – galaxy luminosity*

The $M_{\rm BH}-L_{\rm gal}$ diagram is shown in Figure 1. Four spiral galaxies had their total luminosities underestimated (see Table 1) and thus are not included in the linear regression analysis (see Table 2).

Läsker et al. (2014b) analyzed a sample of 35 galaxies, among which only four were classified as spiral galaxies, and claimed that the $M_{\rm BH} - L_{\rm sph}$ and $M_{\rm BH} - L_{\rm gal}$ relations, which they fit with a single power-law, have consistent intrinsic scatter. Here, instead, thanks to our galaxy sample that includes 17 spiral galaxies, we show that the claim made by Läsker et al. (2014b) is valid only for early-type galaxies. That is, when considering only early-type galaxies, we find that the $M_{\rm BH} - L_{\rm sph}$ and $M_{\rm BH} - L_{\rm gal}$ relations have the same level of intrinsic scatter. However, our $M_{\rm BH} - L_{\rm sph}$ relation for all 66 galaxies, irrespective of their morphological type, has an intrinsic scatter $\epsilon_{(Y|X)} = 0.51 \pm 0.06$ dex (forward linear regression) and $\epsilon_{(X|Y)} = 0.60 \pm 0.09$ dex (inverse linear regression), whereas our $M_{\rm BH} - L_{\rm gal}$ relation for 62 ($= 66 - 4$) galaxies has $\epsilon_{(Y|X)} = 0.63 \pm 0.07$ dex and $\epsilon_{(X|Y)} = 0.91 \pm 0.17$ dex. Because the value of the intrinsic scatter depends on the size of the uncertainties associated with the absolute magnitudes[9], we tested the robustness of our conclusion by increasing the uncertainties associated with the galaxy absolute magnitudes (we originally assumed 0.25 mag). The intrinsic scatter of the $M_{\rm BH} - L_{\rm gal}$ relation only becomes smaller than that of the $M_{\rm BH}-L_{\rm sph}$ relation when assuming an uncertainty larger than 0.7 mag for $L_{\rm gal}$, which would be significantly larger than the typical value commonly recognized in the literature, and would also oddly exceed the typical uncertainty that we estimated for $L_{\rm sph}$. Hence, we conclude that our determination of the relative intrinsic scatter is reliable, and that $M_{\rm BH}$ correlates equally well with $L_{\rm sph}$ and $L_{\rm gal}$ only for early-type galaxies, but not for all (early+late-type) galaxies.

4.2. *Black hole mass – spheroid luminosity*

The $M_{\rm BH} - L_{\rm sph}$ diagram is shown in Figure 2, and the linear regression analysis is presented in Table 3. Sérsic and core-Sérsic spheroids have slopes consistent with each other (within their 1σ uncertainties), in disagreement with the findings of GS13. The slope that we obtained for core-Sérsic spheroids ($M_{\rm BH} \propto L_{\rm sph}^{1.18\pm0.20}$) is consistent with the slope reported by GS13 in the K_s-band for the same population ($M_{\rm BH} \propto L_{\rm sph}^{1.10\pm0.20}$). However, the slope that we determined for Sérsic spheroids ($M_{\rm BH} \propto L_{\rm sph}^{1.53\pm0.20}$) is notably shallower than that found by GS13 ($M_{\rm BH} \propto L_{\rm sph}^{2.73\pm0.55}$).

Although the Sérsic/core-Sérsic classification used by GS13 slightly differs[10] from the classification used here,

---

[7] These are integrated $[3.6]-[4.5]$ colors, measured in a circular aperture within each galaxy's effective radius.
[8] These four cases are discussed in *Paper I*.

[9] The smaller (larger) the uncertainties, the larger (smaller) the intrinsic scatter.
[10] The classification has changed for the galaxies NGC 1316, NGC 1332 and NGC 3998.

Savorgnan et al.

TABLE 1
Galaxy sample.

Galaxy	Type	Core	Distance [Mpc]	M_{BH} [10^8 M$_\odot$]	MAG_{sph} [mag]	MAG_{gal} [mag]	$[3.6]-[4.5]$ [mag]	$M_{*,\mathrm{sph}}$ [10^{10} M$_\odot$]
(1)	(2)	(3)	(4)	(5)	(6)	(7)	(8)	(9)
IC 1459	E	yes	28.4	24^{+10}_{-10}	$-26.15^{+0.18}_{-0.11}$	-26.15 ± 0.25	-0.12	27^{+30}_{-23}
IC 2560	Sp (bar)	no?	40.7	$0.044^{+0.044}_{-0.022}$	$-22.27^{+0.66}_{-0.58}$	-24.76 ± 0.25	-0.08	$1.0^{+1.8}_{-0.6}$
IC 4296	E	yes?	40.7	11^{+2}_{-2}	$-26.35^{+0.18}_{-0.11}$	-26.35 ± 0.25	-0.12	31^{+34}_{-26}
M104	S0/Sp	yes	9.5	$6.4^{+0.4}_{-0.4}$	$-23.91^{+0.66}_{-0.58}$	-25.21 ± 0.25	-0.12	$3.4^{+5.8}_{-1.9}$
M105	E	yes	10.3	4^{+1}_{-1}	$-24.29^{+0.66}_{-0.58}$	-24.29 ± 0.25	-0.10	$5.6^{+9.5}_{-3.0}$
M106	Sp (bar)	no	7.2	$0.39^{+0.01}_{-0.01}$	$-21.11^{+0.18}_{-0.11}$	-24.04 ± 0.25	-0.08	$0.37^{+0.41}_{-0.31}$
M31	Sp (bar)	no	0.7	$1.4^{+0.9}_{-0.3}$	$-22.74^{+0.18}_{-0.11}$	-24.67 ± 0.25	-0.09	$1.5^{+1.6}_{-1.3}$
M49	E	yes	17.1	25^{+3}_{-1}	$-26.54^{+0.18}_{-0.11}$	-26.54 ± 0.25	-0.12	39^{+43}_{-33}
M59	E	no	17.8	$3.9^{+0.4}_{-0.4}$	$-25.18^{+0.18}_{-0.11}$	-25.27 ± 0.25	-0.09	14^{+15}_{-11}
M64	Sp	no?	7.3	$0.016^{+0.004}_{-0.004}$	$-21.54^{+0.18}_{-0.11}$	-24.24 ± 0.25	-0.06	$0.64^{+0.71}_{-0.55}$
M81	Sp (bar)	no	3.8	$0.74^{+0.21}_{-0.11}$	$-23.01^{+0.88}_{-0.66}$	-24.43 ± 0.25	-0.09	$1.9^{+3.6}_{-0.9}$
M84	E	yes	17.9	$9.0^{+0.9}_{-0.8}$	$-26.01^{+0.66}_{-0.58}$	-26.01 ± 0.25	-0.10	28^{+47}_{-15}
M87	E	yes	15.6	$58.0^{+3.5}_{-3.5}$	$-26.00^{+0.66}_{-0.58}$	-26.00 ± 0.25	-0.11	26^{+44}_{-14}
M89	E	yes	14.9	$4.7^{+0.5}_{-0.5}$	$-24.48^{+0.66}_{-0.58}$	-24.74 ± 0.25	-0.11	$6.3^{+10.7}_{-3.4}$
M94	Sp (bar)	no?	4.4	$0.060^{+0.014}_{-0.014}$	$-22.08^{+0.18}_{-0.11}$	≤ -23.36	-0.07	$1.00^{+1.11}_{-0.85}$
M96	Sp (bar)	no	10.1	$0.073^{+0.015}_{-0.015}$	$-22.15^{+0.18}_{-0.11}$	-24.20 ± 0.25	-0.08	$0.97^{+1.08}_{-0.83}$
NGC 0524	S0	yes	23.3	$8.3^{+2.7}_{-1.3}$	$-23.19^{+0.18}_{-0.11}$	-24.92 ± 0.25	-0.09	$2.2^{+2.5}_{-1.9}$
NGC 0821	E	no	23.4	$0.39^{+0.26}_{-0.09}$	$-24.00^{+0.88}_{-0.66}$	-24.26 ± 0.25	-0.09	$4.7^{+8.7}_{-2.1}$
NGC 1023	S0 (bar)	no	11.1	$0.42^{+0.04}_{-0.04}$	$-22.82^{+0.18}_{-0.11}$	-24.20 ± 0.25	-0.10	$1.5^{+1.7}_{-1.3}$
NGC 1300	Sp (bar)	no	20.7	$0.73^{+0.69}_{-0.35}$	$-22.06^{+0.66}_{-0.58}$	-24.16 ± 0.25	-0.10	$0.70^{+1.19}_{-0.38}$
NGC 1316	merger	no	18.6	$1.50^{+0.75}_{-0.80}$	$-24.89^{+0.66}_{-0.58}$	-26.48 ± 0.25	-0.10	$9.5^{+16.2}_{-5.2}$
NGC 1332	E/S0	no	22.3	14^{+2}_{-2}	$-24.89^{+0.88}_{-0.66}$	-24.95 ± 0.25	-0.12	$8.2^{+15.0}_{-3.6}$
NGC 1374	E	no?	19.2	$5.8^{+0.5}_{-0.5}$	$-23.68^{+0.18}_{-0.11}$	-23.70 ± 0.25	-0.09	$3.6^{+4.0}_{-3.0}$
NGC 1399	E	yes	19.4	$4.7^{+0.6}_{-0.6}$	$-26.43^{+0.18}_{-0.11}$	-26.46 ± 0.25	-0.12	33^{+37}_{-28}
NGC 2273	Sp (bar)	no	28.5	$0.083^{+0.004}_{-0.004}$	$-23.00^{+0.66}_{-0.58}$	-24.21 ± 0.25	-0.08	$2.0^{+3.4}_{-1.1}$
NGC 2549	S0 (bar)	no	12.3	$0.14^{+0.02}_{-0.13}$	$-21.25^{+0.18}_{-0.11}$	-22.60 ± 0.25	-0.10	$0.35^{+0.39}_{-0.30}$
NGC 2778	S0 (bar)	no	22.3	$0.15^{+0.09}_{-0.10}$	$-20.80^{+0.66}_{-0.58}$	-22.44 ± 0.25	-0.09	$0.25^{+0.43}_{-0.14}$
NGC 2787	S0 (bar)	no	7.3	$0.40^{+0.04}_{-0.05}$	$-20.11^{+0.66}_{-0.58}$	-22.28 ± 0.25	-0.10	$0.12^{+0.20}_{-0.07}$
NGC 2974	Sp (bar)	no	20.9	$1.7^{+0.2}_{-0.2}$	$-22.95^{+0.66}_{-0.58}$	-24.16 ± 0.25	-0.09	$1.8^{+3.1}_{-1.0}$
NGC 3079	Sp (bar)	no?	20.7	$0.024^{+0.024}_{-0.012}$	$-23.01^{+0.66}_{-0.58}$	≤ -24.45	-0.07	$2.4^{+4.0}_{-1.3}$
NGC 3091	E	yes	51.2	36^{+1}_{-2}	$-26.28^{+0.18}_{-0.11}$	-26.28 ± 0.25	-0.12	30^{+34}_{-26}
NGC 3115	E/S0	no	9.4	$8.8^{+10.0}_{-2.7}$	$-24.22^{+0.18}_{-0.11}$	-24.40 ± 0.25	-0.11	$4.9^{+5.4}_{-4.1}$
NGC 3227	Sp (bar)	no	20.3	$0.14^{+0.10}_{-0.06}$	$-21.76^{+0.66}_{-0.58}$	-24.26 ± 0.25	-0.08	$0.67^{+1.15}_{-0.37}$
NGC 3245	S0 (bar)	no	20.3	$2.0^{+0.5}_{-0.5}$	$-22.43^{+0.18}_{-0.11}$	-23.88 ± 0.25	-0.10	$1.0^{+1.1}_{-0.9}$
NGC 3377	E	no	10.9	$0.77^{+0.04}_{-0.06}$	$-23.49^{+0.66}_{-0.58}$	-23.57 ± 0.25	-0.06	$4.0^{+6.8}_{-2.2}$
NGC 3384	S0 (bar)	no	11.3	$0.17^{+0.01}_{-0.02}$	$-22.43^{+0.18}_{-0.11}$	-23.74 ± 0.25	-0.08	$1.2^{+1.3}_{-1.0}$
NGC 3393	Sp (bar)	no	55.2	$0.34^{+0.02}_{-0.02}$	$-23.48^{+0.66}_{-0.58}$	-25.29 ± 0.25	-0.10	$2.8^{+4.7}_{-1.5}$
NGC 3414	E	no	24.5	$2.4^{+0.3}_{-0.3}$	$-24.35^{+0.18}_{-0.11}$	-24.42 ± 0.25	-0.09	$6.5^{+7.2}_{-5.5}$
NGC 3489	S0/Sp (bar)	no	11.7	$0.058^{+0.008}_{-0.008}$	$-21.13^{+0.66}_{-0.58}$	-23.07 ± 0.25	-0.06	$0.42^{+0.72}_{-0.23}$
NGC 3585	E	no	19.5	$3.1^{+1.4}_{-0.6}$	$-25.52^{+0.66}_{-0.58}$	-25.55 ± 0.25	-0.10	18^{+30}_{-10}
NGC 3607	E	no	22.2	$1.3^{+0.5}_{-0.5}$	$-25.36^{+0.66}_{-0.58}$	-25.45 ± 0.25	-0.10	15^{+25}_{-8}
NGC 3608	E	yes	22.3	$2.0^{+1.1}_{-0.6}$	$-24.50^{+0.66}_{-0.58}$	-24.50 ± 0.25	-0.08	$7.8^{+13.4}_{-4.3}$
NGC 3842	E	yes	98.4	97^{+30}_{-26}	$-27.00^{+0.18}_{-0.11}$	-27.04 ± 0.25	-0.11	61^{+68}_{-52}
NGC 3998	S0 (bar)	no	13.7	$8.1^{+2.0}_{-1.9}$	$-22.32^{+0.88}_{-0.66}$	-23.53 ± 0.25	-0.12	$0.78^{+1.43}_{-0.35}$
NGC 4026	S0 (bar)	no	13.2	$1.8^{+0.6}_{-0.3}$	$-21.58^{+0.88}_{-0.66}$	-23.16 ± 0.25	-0.09	$0.50^{+0.92}_{-0.22}$
NGC 4151	Sp (bar)	no	20.0	$0.65^{+0.07}_{-0.07}$	$-23.40^{+0.66}_{-0.58}$	-24.44 ± 0.25	-0.09	$2.8^{+4.8}_{-1.5}$
NGC 4261	E	yes	30.8	5^{+1}_{-1}	$-25.72^{+0.66}_{-0.58}$	-25.76 ± 0.25	-0.12	18^{+30}_{-10}
NGC 4291	E	yes	25.5	$3.3^{+0.9}_{-2.5}$	$-24.05^{+0.66}_{-0.58}$	-24.05 ± 0.25	-0.11	$3.9^{+6.7}_{-2.1}$
NGC 4388	Sp (bar)	no?	17.0	$0.075^{+0.002}_{-0.002}$	$-21.26^{+0.88}_{-0.66}$	≤ -23.50	-0.07	$0.46^{+0.85}_{-0.21}$
NGC 4459	S0	no	15.7	$0.68^{+0.13}_{-0.13}$	$-23.48^{+0.66}_{-0.58}$	-24.01 ± 0.25	-0.09	$2.9^{+5.0}_{-1.6}$
NGC 4473	E	no	15.3	$1.2^{+0.4}_{-0.9}$	$-23.88^{+0.66}_{-0.58}$	-24.11 ± 0.25	-0.10	$3.9^{+6.6}_{-2.1}$
NGC 4564	S0	no	14.6	$0.60^{+0.03}_{-0.09}$	$-22.30^{+0.18}_{-0.11}$	-22.99 ± 0.25	-0.11	$0.82^{+0.91}_{-0.70}$
NGC 4596	S0 (bar)	no	17.0	$0.79^{+0.38}_{-0.33}$	$-22.73^{+0.18}_{-0.11}$	-24.18 ± 0.25	-0.08	$1.6^{+1.7}_{-1.3}$

Galaxy	Type	Core	Distance [Mpc]	$M_{\rm BH}$ [10^8 M$_\odot$]	$MAG_{\rm sph}$ [mag]	$MAG_{\rm gal}$ [mag]	$[3.6] - [4.5]$ [mag]	$M_{\rm *,sph}$ [10^{10} M$_\odot$]
(1)	(2)	(3)	(4)	(5)	(6)	(7)	(8)	(9)
NGC 4697	E	no	11.4	$1.8^{+0.2}_{-0.1}$	$-24.82^{+0.88}_{-0.66}$	-24.94 ± 0.25	-0.09	10^{+18}_{-4}
NGC 4889	E	yes	103.2	210^{+160}_{-160}	$-27.54^{+0.18}_{-0.11}$	-27.54 ± 0.25	-0.12	91^{+101}_{-77}
NGC 4945	Sp (bar)	no?	3.8	$0.014^{+0.014}_{-0.007}$	$-20.96^{+0.66}_{-0.58}$	≤ -23.79	-0.06	$0.36^{+0.62}_{-0.20}$
NGC 5077	E	yes	41.2	$7.4^{+4.7}_{-3.0}$	$-25.45^{+0.18}_{-0.11}$	-25.45 ± 0.25	-0.11	15^{+17}_{-13}
NGC 5128	merger	no?	3.8	$0.45^{+0.17}_{-0.10}$	$-23.89^{+0.88}_{-0.66}$	-24.97 ± 0.25	-0.07	$5.0^{+9.1}_{-2.2}$
NGC 5576	E	no	24.8	$1.6^{+0.3}_{-0.4}$	$-24.44^{+0.18}_{-0.11}$	-24.44 ± 0.25	-0.09	$7.1^{+7.9}_{-6.0}$
NGC 5845	S0	no	25.2	$2.6^{+0.4}_{-1.5}$	$-22.96^{+0.88}_{-0.66}$	-23.10 ± 0.25	-0.12	$1.4^{+2.6}_{-0.6}$
NGC 5846	E	yes	24.2	11^{+1}_{-1}	$-25.81^{+0.66}_{-0.58}$	-25.81 ± 0.25	-0.10	22^{+38}_{-12}
NGC 6251	E	yes?	104.6	5^{+2}_{-2}	$-26.75^{+0.18}_{-0.11}$	-26.75 ± 0.25	-0.12	46^{+51}_{-39}
NGC 7052	E	yes	66.4	$3.7^{+2.6}_{-1.5}$	$-26.32^{+0.18}_{-0.11}$	-26.32 ± 0.25	-0.11	33^{+36}_{-28}
NGC 7619	E	yes	51.5	25^{+8}_{-3}	$-26.35^{+0.66}_{-0.58}$	-26.41 ± 0.25	-0.11	33^{+56}_{-18}
NGC 7768	E	yes	112.8	13^{+5}_{-4}	$-26.90^{+0.66}_{-0.58}$	-26.90 ± 0.25	-0.11	57^{+98}_{-31}
UGC 03789	Sp (bar)	no?	48.4	$0.108^{+0.005}_{-0.005}$	$-22.77^{+0.88}_{-0.66}$	-24.20 ± 0.25	-0.07	$1.9^{+3.4}_{-0.8}$

NOTE. — *Column (1)*: Galaxy name. *Column (2)*: Morphological type (E=elliptical, S0=lenticular, Sp=spiral, merger). The morphological classification of four galaxies is uncertain (E/S0 or S0/Sp). The presence of a bar is indicated. *Column (3)*: Presence of a partially depleted core. The question mark is used when the classification has come from the velocity dispersion criteria mentioned in Section 2. *Column (4)*: Distance. *Column (5)*: Black hole mass. *Column (6)*: Absolute 3.6 μm bulge magnitude. Bulge magnitudes come from our state-of-the-art multicomponent galaxy decompositions (*Paper I*), which include bulges, disks, bars, spiral arms, rings, haloes, extended or unresolved nuclear sources and partially depleted cores, and that – for the first time – were checked to be consistent with the galaxy kinematics. The uncertainties were estimated with a method that takes into account systematic errors, which are typically not considered by popular 2D fitting codes. *Column (7)*: Absolute 3.6 μm galaxy magnitude. Four galaxies had their magnitudes overestimated, which are given here as upper limits. *Column (8)*: $[3.6] - [4.5]$ colour. *Column (9)*: Bulge stellar mass.

TABLE 2
LINEAR REGRESSION ANALYSIS OF THE $M_{\rm BH} - L_{\rm gal}$ DIAGRAM.

Subsample (size)	Regression	α	β	$\langle MAG_{\rm gal}\rangle$	ϵ	Δ
	$\log[M_{\rm BH}/{\rm M}_\odot] = \alpha + \beta[(MAG_{\rm gal} - \langle MAG_{\rm gal}\rangle)/{\rm mag}]$					
All (62)	BCES $(Y|X)$	8.26 ± 0.08	-0.49 ± 0.06	-24.78	–	0.64
	BCES $(X|Y)$	8.26 ± 0.12	-1.01 ± 0.15	-24.78	–	0.92
	BCES Bisector	8.26 ± 0.09	-0.72 ± 0.07	-24.78	–	0.71
	mFITEXY $(Y|X)$	$8.26^{+0.08}_{-0.08}$	$-0.49^{+0.06}_{-0.07}$	-24.78	$0.61^{+0.07}_{-0.06}$	0.64
	mFITEXY $(X|Y)$	$8.26^{+0.11}_{-0.12}$	$-1.03^{+0.13}_{-0.16}$	-24.78	$0.88^{+0.10}_{-0.08}$	0.93
	mFITEXY Bisector	$8.26^{+0.10}_{-0.10}$	$-0.73^{+0.09}_{-0.10}$	-24.78	–	0.71
	linmix_err $(Y|X)$	8.26 ± 0.09	-0.49 ± 0.07	-24.78	0.63 ± 0.07	0.64
	linmix_err $(X|Y)$	8.26 ± 0.12	-1.02 ± 0.15	-24.78	0.91 ± 0.17	0.93
	linmix_err Bisector	8.26 ± 0.10	-0.72 ± 0.15	-24.78	–	0.71
Early-type (E+S0) (45)	BCES $(Y|X)$	8.56 ± 0.07	-0.44 ± 0.05	-24.88	–	0.45
	BCES $(X|Y)$	8.56 ± 0.08	-0.64 ± 0.05	-24.88	–	0.53
	BCES Bisector	8.56 ± 0.07	-0.53 ± 0.04	-24.88	–	0.47
	mFITEXY $(Y|X)$	$8.56^{+0.06}_{-0.06}$	$-0.42^{+0.05}_{-0.05}$	-24.88	$0.41^{+0.06}_{-0.05}$	0.45
	mFITEXY $(X|Y)$	$8.56^{+0.08}_{-0.08}$	$-0.66^{+0.07}_{-0.08}$	-24.88	$0.51^{+0.07}_{-0.06}$	0.55
	mFITEXY Bisector	$8.56^{+0.07}_{-0.07}$	$-0.54^{+0.06}_{-0.06}$	-24.88	–	0.47
	linmix_err $(Y|X)$	8.56 ± 0.07	-0.42 ± 0.06	-24.88	0.43 ± 0.06	0.45
	linmix_err $(X|Y)$	8.56 ± 0.09	-0.65 ± 0.08	-24.88	0.53 ± 0.10	0.54
	linmix_err Bisector	8.56 ± 0.08	-0.53 ± 0.10	-24.88	–	0.47

NOTE. — For each subsample, we indicate $\langle MAG_{\rm gal}\rangle$, its average value of galaxy magnitudes. In the last two columns, we report ϵ, the intrinsic scatter, and Δ, the total rms scatter in the $\log(M_{\rm BH})$ direction. Four spiral galaxies had their luminosities underestimated and thus are not included in the linear regression analysis (the sample of all galaxies contains 66-4=62 objects). When considering all galaxies, irrespective of their morphological type, the $M_{\rm BH} - L_{\rm gal}$ correlation is weaker than the $M_{\rm BH} - L_{\rm sph}$ correlation, in terms of intrinsic scatter. However, when considering only early-type galaxies, the $M_{\rm BH} - L_{\rm gal}$ and $M_{\rm BH} - L_{\rm sph}$ correlations have consistent intrinsic scatter.
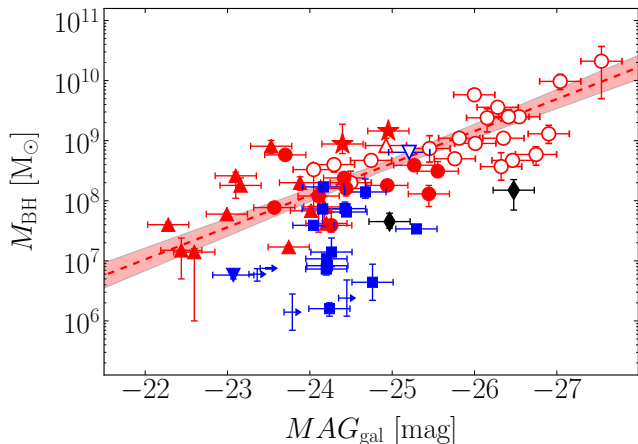
FIG. 1.— Black hole mass plotted against 3.6 μm galaxy absolute magnitude. Symbols are coded according to the galaxy morphological type: red circle = E, red star = E/S0, red upward triangle = S0, blue downward triangle = S0/Sp, blue square = Sp, black diamond = merger. Empty symbols represent core-Sérsic spheroids, whereas filled symbols are used for Sérsic spheroids. Four spiral galaxies had their magnitudes overestimated (luminosities underestimated) and are shown as upper limits. The red dashed line indicates the BCES bisector linear regression for the 45 early-type galaxies (E+S0), with the red shaded area denoting its 1σ uncertainty. M_{BH} correlates equally well with L_{gal} and L_{sph} only for early-type galaxies, but not for all (early+late-type) galaxies.

the main cause of the inconsistency is that the bulge-to-total ratios obtained from our galaxy decompositions are different from those assumed by GS13 to convert galaxy luminosities into bulge luminosities. Our bulge-to-total ratios for low-luminosity Sérsic spheroids (3.6 μm $MAG_{sph} \gtrsim -22$ mag) are smaller than those used by GS13. The host galaxies of such bulges are late-type, spiral galaxies, which typically present a complex morphology (bars, double bars, embedded disks, nuclear components, etc). Our galaxy models account for the extra components, while the average bulge-to-total ratios of GS13 were based on less sophisticated Sérsic-bulge/exponential-disk decompositions which overestimated the bulge luminosity. This results in our bulge magnitudes being on average ~0.7 mag fainter than in GS13, after accounting for the different wavelength of the data. At the same time, our bulge-to-total ratios for the high-luminosity Sérsic spheroids (3.6 μm $MAG_{sph} \lesssim -24$ mag) are on average larger than those adopted by GS13. In this regime, the host systems are early-type galaxies that feature intermediate-scale disks[11]. Past bulge/disk decompositions failed to correctly identify the extent of such disks and treated them as large-scale disks, thus underestimating the bulge luminosity. The magnitudes that we obtained for such spheroids are on average ~0.5 mag brighter than in GS13. These two effects explain the shallower slope that we obtained for the Sérsic spheroids.

[11] Intermediate-scale disks are disks of stars fully embedded in the spheroidal component of their galaxy. They are typical of "disky" elliptical galaxies (e.g. NGC 3377), but they can also be found in other types of host galaxies. They can be considered an intermediate class between nuclear disks, with sizes ~10 − 100 pc, and large-scale disks, that encase the bulge and dominate the light at large radii.

The slope that we obtained for Sérsic spheroids (1.53 ± 0.20) is not consistent with the value of 2.5 expected from $M_{BH} \propto \sigma^5$ and $L_{sph} \propto \sigma^2$. In addition, the Sérsic and core-Sérsic spheroids appear not to define two distinct $M_{BH} - L_{sph}$ sequences. This leads us to investigate substructure in the $M_{BH} - L_{sph}$ diagram for early- and late-type galaxies. First, we checked that the elliptical and lenticular galaxies, taken separately, have slopes consistent with each other, and thus, taken together, they define a single *early-type sequence* in the $M_{BH} - L_{sph}$ diagram. We then fit the early-type galaxies with a single log-linear regression, and obtained $M_{BH} \propto L_{sph}^{1.00\pm0.10}$. We did not find any convincing evidence for the change in slope required for consistency with the $M_{BH} - \sigma$ and bent $L_{sph} - \sigma$ correlations. Because the change in slope should occur at $M_{BH} > 10^{8\pm1}$ M$_\odot$, but all the early-type galaxies in our sample have $M_{BH} \gtrsim 10^7$ M$_\odot$, one possible explanation is that we are still not probing enough low black hole masses for this subsample. An additional possibility is that there is no sharp transition going from $L_{sph} \propto \sigma^2$ at low luminosities to $L_{sph} \propto \sigma^5$ at high luminosities. Although the knowledge that many "elliptical" galaxies actually contain embedded stellar disks dates back at least three decades (Capaccioli 1987; Carter 1987; Rix & White 1990; Bender 1990; Scorza & Bender 1990; Nieto et al. 1991; Rix & White 1992; Scorza & Bender 1995), it is mainly thanks to large integral-field-spectrograph surveys of early-type galaxies, such as the ATLAS^{3D} Project (Cappellari et al. 2011), that our view has been further advanced and it is now commonly accepted that most "elliptical" galaxies contain disks. Past studies that investigated the $L_{sph}-\sigma$ diagram might have failed to identify and consequently model the disks in intermediate-luminosity, early-type galaxies, thus overestimating L_{sph} and mistakenly producing a sharp bend in the $L_{sph} - \sigma$ correlation, rather than a continuously curved relation (with $L_{sph} \propto \sigma^{3-4}$ at intermediate luminosities).

For the bulges of late-type galaxies we obtained $M_{BH} \propto L_{sph}^{2.88\pm0.68}$. From a cursory inspection of Figure 2, one might be tempted to doubt the statistical significance of this "tentative" *late-type sequence*. However, a visual inspection of the plotted data requires one to take into account the error bars when judging-by-eye the strength of a correlation. Similarly, the Pearson's and Spearman's correlation coefficients are not applicable because they do not take into account the error bars on our data. We have therefore relied on the quantitative regression analysis.

4.2.1. *Pseudo- versus classical bulges*

Current views distinguish between classical bulges (which are considered to be spheroidal, pressure-supported systems, formed through violent processes, such as hierarchical clustering via minor mergers), and pseudo-bulges (thought to be disk-like, rotation-supported systems, built from secular evolution processes, such as instabilities of their surrounding disk or bar). Pseudo-bulges are notoriously hard to identify (Graham 2013, 2014, 2015a,c). For example, mergers can create bulges that rotate (e.g. Bekki 2010; Keselman & Nusser 2012), and bars can spin-up classical bulges (e.g. Saha et al. 2012), thus rotation is not a definitive signature of a pseudo-bulge. Furthermore, many galax-

ies host both a classical and a pseudo-bulge (e.g. Erwin et al. 2003, 2015; Athanassoula 2005; Gadotti 2009; MacArthur et al. 2009; dos Anjos & da Silva 2013; Seidel et al. 2015). In the recent literature, pseudo- and classical bulges have frequently been divided at the Sérsic index $n_{\rm sph} = 2$ (e.g. Sani et al. 2011; Beifiori et al. 2012), although, from a selection of hundreds of disc galaxies imaged in the K-band, Graham & Worley (2008) observed no bimodality in the bulge Sérsic indices about $n_{\rm sph} = 2$ or any other value. While pseudo-bulges are expected to have exponential-like surface brightness profiles ($n_{\rm sph} \simeq 1$), being disky components that formed from their surrounding exponential disks (e.g. Bardeen 1975; Hohl 1975; Combes & Sanders 1981; Combes et al. 1990; Pfenniger & Friedli 1991), it has been shown that mergers can create bulges with $n_{\rm sph} < 2$ (e.g. Eliche-Moral et al. 2011; Scannapieco et al. 2011; Querejeta et al. 2015), just as low-luminosity elliptical galaxies (not built from the secular evolution of a disk) are also well known to have $n_{\rm sph} < 2$ and even $n_{\rm sph} < 1$ (e.g. Davies et al. 1988; Young & Currie 1994; Jerjen et al. 2000). The use of the Sérsic index (in addition to rotation) to identify pseudo-bulges is thus a dangerous practice.

Sani et al. (2011) reported that pseudo-bulges – which they labelled as such according to the $n_{\rm sph} < 2$ criterion – with low black hole masses ($M_{\rm BH} < 10^7$ M$_\odot$) are significantly displaced from the correlation traced by their (classical) bulges with $n_{\rm sph} > 2$. In Figure 3, we show the distribution of spheroid Sérsic indices[12] in the $M_{\rm BH} - L_{\rm sph}$ diagram. Our aim is to check whether bulges with $n_{\rm sph} < 2$ are offset to lower black hole masses from the correlation defined by bulges with $n_{\rm sph} > 2$. To do this, we fit a symmetrical linear regression to the bulges that have $n_{\rm sph} > 2$ and we then compute the vertical offset of all bulges from this regression. In Figure 3, we plot the vertical offset against $n_{\rm sph}$. Among the 23 bulges with $n_{\rm sph} < 2$, 12 have a positive vertical offset and 11 have a negative vertical offset. Kormendy (2015) provides a list of many pseudo-bulge classification criteria, including the divide at $n_{\rm sph} = 2$, and cautions that each individual criterion has a failure rate of 0-25%. If this is true, we should have that no less than 75% of bulges with $n_{\rm sph} < 2$ display a negative vertical offset[13]. What we observe, instead, is that there are the same number of bulges with $n_{\rm sph} < 2$ lying above and below the correlation defined by bulges with $n_{\rm sph} > 2$, and that the amplitude of their offset is the same ($\lesssim 1.5$ dex). That is, bulges with $n_{\rm sph} < 2$ do not appear to be offset from the correlation traced by bulges with $n_{\rm sph} > 2$.

4.3. Black hole mass – spheroid stellar mass

Finally, we present the $M_{\rm BH} - M_{*,\rm sph}$ diagram in Figure 5, and its linear regression analysis in Table 4. The bulges of the early-type galaxies follow $M_{\rm BH} \propto M_{*,\rm sph}^{1.04\pm0.10}$, consistent with a dry-merging formation sce-

----

[12] The spheroid Sérsic indices are taken from our galaxy decompositions (*Paper I*).

[13] One reaches the same conclusion when using the vertical offset from the correlation defined by bulges with $n_{\rm sph} > 3$ or even $n_{\rm sph} > 4$. There are 13 and 10 bulges with $n_{\rm sph} < 2$ that lie above and below, respectively, the correlation traced by bulges with $n_{\rm sph} > 3$. Similarly, there are 15 and 8 bulges with $n_{\rm sph} < 2$ that lie above and below, respectively, the correlation traced by bulges with $n_{\rm sph} > 4$.
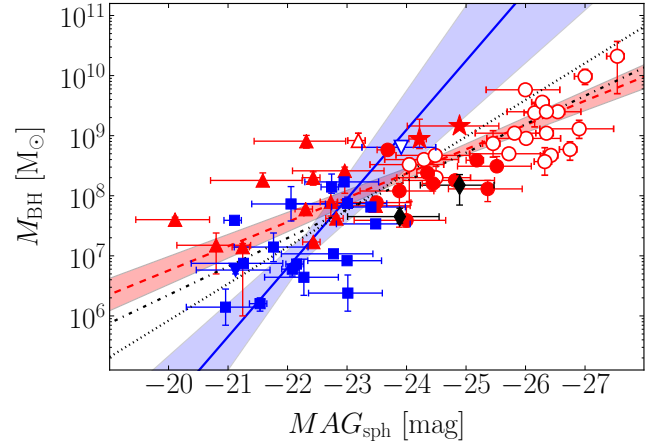

FIG. 2.— Black hole mass plotted against 3.6 μm spheroid absolute magnitude. Symbols have the same meaning as in Figure 1. The red dashed line indicates the BCES bisector linear regression for the spheroidal component of the 45 early-type (E+S0) galaxies, with the red shaded area denoting its 1σ uncertainty. The blue solid line shows the BCES bisector linear regression for the bulges of the 17 late-type (Sp) galaxies, with the blue shaded area denoting its 1σ uncertainty. The black dashed-dotted and dotted lines represent the BCES bisector linear regressions for the core-Sérsic and Sérsic spheroids, respectively.
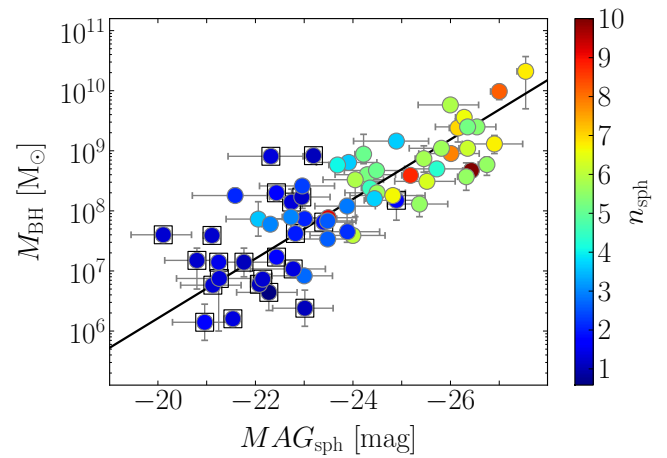

FIG. 3.— Black hole mass plotted against 3.6 μm spheroid absolute magnitude. Symbols are color coded according to the spheroid Sérsic index $n_{\rm sph}$. Bulges with $n_{\rm sph} < 2$, claimed by some to be pseudo-bulges, are enclosed with a square. The black solid line shows the BCES bisector linear regression for the spheroids that have $n_{\rm sph} \geq 2$, such that $M_{\rm BH} \propto L_{\rm sph}^{1.25\pm0.13}$.

nario, and define a tight *early-type sequence* with intrinsic scatter $\epsilon_{(Y|X)} = 0.43\pm0.06$ dex. Graham (2012) reported that the $M_{\rm BH}/M_{\rm dyn,sph}$ ratio for core-Sérsic galaxies was 0.36% ($M_{\rm dyn,sph}$ is the spheroid dynamical mass), and discussed the many implications of this. Using a larger data sample, Graham & Scott (2013) reported that the $M_{\rm BH}/M_{*,\rm sph}$ ratio was 0.49% for core-Sérsic galaxies. Here we find a median $M_{\rm BH}/M_{*,\rm sph}$ ratio of 0.50±0.04% for the 22 core-Sérsic galaxies and 0.68 ± 0.04% for the 45 early-type galaxies. Among other things, this higher value (previously reported to be $0.1 - 0.2\%$ for all galaxy

Savorgnan et al.

TABLE 3
Linear regression analysis of the $M_{\rm BH} - L_{\rm sph}$ diagram.

Subsample (size)	Regression	α	β	$\langle MAG_{\rm sph} \rangle$	ϵ	Δ
	$\log[M_{\rm BH}/{\rm M_\odot}] = \alpha + \beta[(MAG_{\rm sph} - \langle MAG_{\rm sph}\rangle)/{\rm mag}]$				
All (66)	BCES $(Y\|X)$	8.16 ± 0.07	-0.44 ± 0.04	-23.86	$-$	0.56
	BCES $(X\|Y)$	8.16 ± 0.08	-0.61 ± 0.05	-23.86	$-$	0.68
	BCES Bisector	8.16 ± 0.07	-0.52 ± 0.04	-23.86	$-$	0.60
	mFITEXY $(Y\|X)$	$8.17^{+0.06}_{-0.07}$	$-0.43^{+0.03}_{-0.04}$	-23.86	$0.49^{+0.06}_{-0.05}$	0.56
	mFITEXY $(X\|Y)$	$8.15^{+0.07}_{-0.08}$	$-0.61^{+0.05}_{-0.05}$	-23.86	$0.58^{+0.07}_{-0.06}$	0.68
	mFITEXY Bisector	$8.16^{+0.07}_{-0.07}$	$-0.51^{+0.04}_{-0.04}$	-23.86	$-$	0.60
	linmix_err $(Y\|X)$	8.16 ± 0.07	-0.42 ± 0.04	-23.86	0.51 ± 0.06	0.56
	linmix_err $(X\|Y)$	8.16 ± 0.09	-0.60 ± 0.06	-23.86	0.60 ± 0.09	0.67
	linmix_err Bisector	8.16 ± 0.08	-0.51 ± 0.09	-23.86	$-$	0.59
$n > 2$ (43)	BCES $(Y\|X)$	8.58 ± 0.07	-0.42 ± 0.06	-24.77	$-$	0.46
	BCES $(X\|Y)$	8.58 ± 0.08	-0.58 ± 0.06	-24.77	$-$	0.56
	BCES Bisector	8.58 ± 0.07	-0.50 ± 0.05	-24.77	$-$	0.49
	mFITEXY $(Y\|X)$	$8.57^{+0.07}_{-0.06}$	$-0.41^{+0.04}_{-0.04}$	-24.77	$0.38^{+0.06}_{-0.06}$	0.46
	mFITEXY $(X\|Y)$	$8.56^{+0.08}_{-0.08}$	$-0.57^{+0.06}_{-0.07}$	-24.77	$0.44^{+0.08}_{-0.11}$	0.55
	mFITEXY Bisector	$8.57^{+0.07}_{-0.07}$	$-0.49^{+0.05}_{-0.05}$	-24.77	$-$	0.49
	linmix_err $(Y\|X)$	8.56 ± 0.07	-0.39 ± 0.05	-24.77	0.40 ± 0.06	0.46
	linmix_err $(X\|Y)$	8.55 ± 0.09	-0.57 ± 0.08	-24.77	0.49 ± 0.10	0.55
	linmix_err Bisector	8.56 ± 0.08	-0.48 ± 0.10	-24.77	$-$	0.49
Core-Sérsic (22)	BCES $(Y\|X)$	9.06 ± 0.09	-0.32 ± 0.11	-25.73	$-$	0.42
	BCES $(X\|Y)$	9.06 ± 0.12	-0.65 ± 0.12	-25.73	$-$	0.61
	BCES Bisector	9.06 ± 0.10	-0.47 ± 0.08	-25.73	$-$	0.48
	mFITEXY $(Y\|X)$	$9.06^{+0.08}_{-0.09}$	$-0.26^{+0.08}_{-0.07}$	-25.73	$0.36^{+0.09}_{-0.06}$	0.42
	mFITEXY $(X\|Y)$	$9.03^{+0.15}_{-0.16}$	$-0.72^{+0.17}_{-0.31}$	-25.73	$0.61^{+0.14}_{-0.09}$	0.68
	mFITEXY Bisector	$9.05^{+0.12}_{-0.13}$	$-0.47^{+0.12}_{-0.17}$	-25.73	$-$	0.48
	linmix_err $(Y\|X)$	9.04 ± 0.10	-0.24 ± 0.09	-25.73	0.40 ± 0.08	0.42
	linmix_err $(X\|Y)$	9.03 ± 0.17	-0.69 ± 0.27	-25.73	0.68 ± 0.30	0.64
	linmix_err Bisector	9.04 ± 0.14	-0.44 ± 0.16	-25.73	$-$	0.46
Sérsic (44)	BCES $(Y\|X)$	7.71 ± 0.09	-0.41 ± 0.08	-22.92	$-$	0.61
	BCES $(X\|Y)$	7.71 ± 0.14	-0.86 ± 0.16	-22.92	$-$	0.93
	BCES Bisector	7.71 ± 0.10	-0.61 ± 0.08	-22.92	$-$	0.71
	mFITEXY $(Y\|X)$	$7.72^{+0.08}_{-0.09}$	$-0.41^{+0.07}_{-0.08}$	-22.92	$0.54^{+0.08}_{-0.07}$	0.61
	mFITEXY $(X\|Y)$	$7.72^{+0.14}_{-0.13}$	$-0.86^{+0.13}_{-0.19}$	-22.92	$0.77^{+0.13}_{-0.10}$	0.93
	mFITEXY Bisector	$7.72^{+0.11}_{-0.11}$	$-0.61^{+0.10}_{-0.12}$	-22.92	$-$	0.71
	linmix_err $(Y\|X)$	7.73 ± 0.09	-0.41 ± 0.08	-22.92	0.55 ± 0.08	0.61
	linmix_err $(X\|Y)$	7.73 ± 0.14	-0.86 ± 0.17	-22.92	0.79 ± 0.20	0.93
	linmix_err Bisector	7.73 ± 0.12	-0.62 ± 0.15	-22.92	$-$	0.71
Early-type (E+S0) (45)	BCES $(Y\|X)$	8.56 ± 0.07	-0.33 ± 0.04	-24.47	$-$	0.46
	BCES $(X\|Y)$	8.56 ± 0.08	-0.48 ± 0.05	-24.47	$-$	0.55
	BCES Bisector	$\mathbf{8.56 \pm 0.07}$	$\mathbf{-0.40 \pm 0.04}$	$\mathbf{-24.47}$	$-$	**0.49**
	mFITEXY $(Y\|X)$	$8.56^{+0.06}_{-0.06}$	$-0.32^{+0.03}_{-0.04}$	-24.47	$0.40^{+0.06}_{-0.05}$	0.46
	mFITEXY $(X\|Y)$	$8.54^{+0.08}_{-0.08}$	$-0.49^{+0.05}_{-0.06}$	-24.47	$0.49^{+0.08}_{-0.06}$	0.57
	mFITEXY Bisector	$8.55^{+0.07}_{-0.07}$	$-0.41^{+0.04}_{-0.05}$	-24.47	$-$	0.49
	linmix_err $(Y\|X)$	8.55 ± 0.07	-0.32 ± 0.04	-24.47	0.41 ± 0.06	0.46
	linmix_err $(X\|Y)$	8.55 ± 0.09	-0.48 ± 0.06	-24.47	0.51 ± 0.10	0.56
	linmix_err Bisector	8.55 ± 0.08	-0.40 ± 0.09	-24.47	$-$	0.49
Late-type (Sp) (17)	BCES $(Y\|X)$	7.18 ± 0.16	-0.79 ± 0.43	-22.33	$-$	0.70
	BCES $(X\|Y)$	7.18 ± 0.29	-1.71 ± 0.71	-22.33	$-$	1.26
	BCES Bisector	$\mathbf{7.18 \pm 0.20}$	$\mathbf{-1.15 \pm 0.27}$	$\mathbf{-22.33}$	$-$	**0.88**
	mFITEXY $(Y\|X)$	$7.20^{+0.15}_{-0.15}$	$-0.53^{+0.22}_{-0.24}$	-22.33	$0.55^{+0.15}_{-0.10}$	0.63
	mFITEXY $(X\|Y)$	$7.38^{+0.54}_{-0.36}$	$-2.02^{+0.71}_{-2.13}$	-22.33	$1.09^{+0.41}_{-0.24}$	1.50
	mFITEXY Bisector	$7.26^{+0.40}_{-0.28}$	$-1.03^{+0.33}_{-0.52}$	-22.33	$-$	0.82
	linmix_err $(Y\|X)$	7.24 ± 0.19	-0.46 ± 0.32	-22.33	0.63 ± 0.16	0.62
	linmix_err $(X\|Y)$	7.34 ± 0.43	-1.93 ± 1.30	-22.33	1.31 ± 0.97	1.43
	linmix_err Bisector	7.27 ± 0.33	-0.96 ± 0.50	-22.33	$-$	0.78

Note. — For each subsample, we indicate $\langle MAG_{\rm sph} \rangle$, its average value of spheroid magnitudes. In the last two columns, we report ϵ, the intrinsic scatter, and Δ, the total rms scatter in the $\log(M_{\rm BH})$ direction. Both the early- and late-type subsamples do not contain the two galaxies classified as S0/Sp and the two galaxies classified as mergers (45+17=66-2-2).
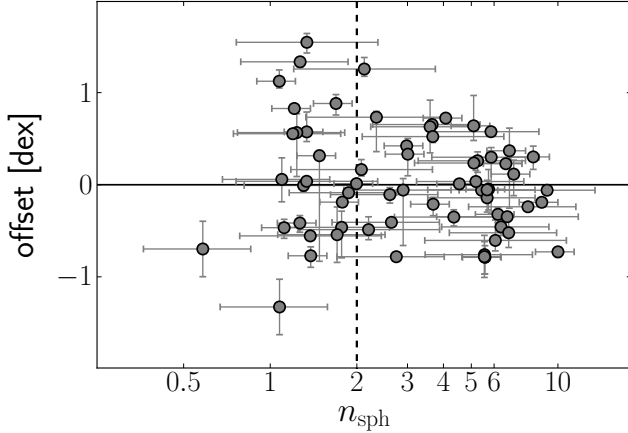
FIG. 4.— Vertical offset from the $M_{\mathrm{BH}} - L_{\mathrm{sph}}$ correlation defined by spheroids with $n_{\mathrm{sph}} \geq 2$ (see Figure 3), plotted against n_{sph}. The vertical dashed line corresponds to $n_{\mathrm{sph}} = 2$. The horizontal solid line is equivalent to a zero vertical offset. Among the bulges with $n_{\mathrm{sph}} < 2$, 12 have a positive vertical offset and 11 have a negative vertical offset. Hence, bulges with $n_{\mathrm{sph}} < 2$ are not randomly offset to lower black hole masses from the correlation traced by bulges with $n_{\mathrm{sph}} \geq 2$.
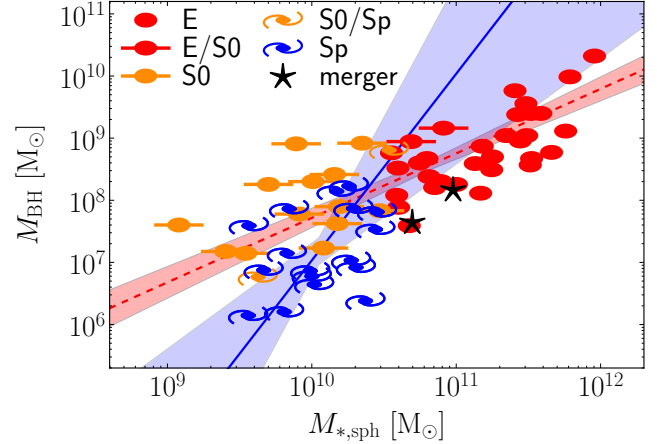

FIG. 5.— Black hole mass plotted against spheroid stellar mass. Symbols are coded according to the galaxy morphological type (see legend). The red dashed line indicates the BCES bisector linear regression for the bulges of the 45 early-type galaxies (E+S0), with the red shaded area denoting its 1σ uncertainty. The bulges of early-type galaxies follow $M_{\mathrm{BH}} \propto M_{*,\mathrm{sph}}^{1.04 \pm 0.10}$, a near-linear relation consistent with a dry-merging formation scenario. The steeper blue solid line shows the BCES bisector linear regression for the bulges of the 17 late-type (Sp) galaxies, with the blue shaded area denoting its 1σ uncertainty. The bulges of late-type galaxies follow $M_{\mathrm{BH}} \propto M_{*,\mathrm{sph}}^{2-3}$, indicating that gas-rich processes feed the black hole more efficiently ("quadratically" or "cubically") than the host bulge grows in stellar mass. We note that AGNs with $10^5 \lesssim M_{\mathrm{BH}}/\mathrm{M}_\odot \lesssim 2 \times 10^6$ (Jiang et al. 2011) appear to follow the blue line (see Graham et al. 2015, *in preparation*).

types, e.g. Marconi & Hunt 2003), boosts estimates of the black hole mass function and mass density based on galaxy/spheroid luminosity functions.

The bulges of the spiral galaxies trace a steeper *late-type sequence*, whose slope is less well constrained due to the smaller size of the subsample and, more importantly, to the smaller range in $M_{*,\mathrm{sph}}$ that the subsample spans. For the bulges of spiral galaxies, the BCES code returns a log-linear relation with a slope = 3.00 ± 1.30, while the modified FITEXY routine finds a shallower (but still consistent within the 1σ uncertainty) slope = $2.28^{+1.67}_{-1.01}$. The Bayesian estimator of Kelly (2007) fails in performing an inverse $(X|Y)$ linear regression for the subsample of spiral galaxies. More data would be welcome to better constrain the slope of this *late-type sequence*, although we note that direct measurements of black hole masses below 10^6 $\mathrm{M}_\odot$ are extremely challenging to obtain with the current technological resources. In this regard, using a sample of ∼140 low-redshift ($z \leq 0.35$, with a median redshift $\langle z \rangle = 0.085$) bulges hosting Active Galactic Nuclei (AGNs) with virial black hole masses $10^5 \lesssim M_{\mathrm{BH}}/\mathrm{M}_\odot \lesssim 2 \times 10^6$ (Jiang et al. 2011), Graham & Scott (2015) showed that they roughly follow the quadratic $M_{\mathrm{BH}} - M_{*,\mathrm{sph}}$ relation defined by their Sérsic bulges. The majority of our spiral galaxies host an AGN[14] and we anticipate here that the correlation traced by our spiral galaxy bulges may track the location of these lower mass AGN in the $M_{\mathrm{BH}} - M_{*,\mathrm{sph}}$ diagram. That is, the AGNs appear to be the low-mass continuation of our tentative *late-type sequence* shown in Figure 5 and this will be explored with more rigour in a forthcoming paper.

5. CONCLUSIONS

Using 3.6 μm *Spitzer* images, we have performed accurate multicomponent decompositions (i.e. bulge, disks, bars, spiral arms, rings, halo, nucleus, depleted core, etc.), which were checked to be consistent with the two-dimensional galaxy kinematics, for 66 nearby galaxies with a dynamical measurement of their black hole mass. We have derived galaxy luminosities, spheroid luminosities and spheroid stellar masses. Our galaxy sample, besides being to date the largest sample with reliable bulge masses used to investigate black hole mass scaling relations, contains 17 spiral galaxies, half of which have $M_{\mathrm{BH}} < 10^7$ $\mathrm{M}_\odot$. This constitutes a significant improvement over past studies whose samples were biased towards high-mass, early-type galaxies.

Using our state-of-the-art dataset, we have investigated substructure in the $M_{\mathrm{BH}} - L_{\mathrm{gal}}$, $M_{\mathrm{BH}} - L_{\mathrm{sph}}$ and $M_{\mathrm{BH}} - M_{*,\mathrm{sph}}$ diagrams. Our principal conclusions are:

- The $M_{\mathrm{BH}} - M_{*,\mathrm{sph}}$ log-relation for the spheroidal components of early-type (elliptical + lenticular) galaxies has a slope of 1.04 ± 0.10 and intrinsic scatter $\epsilon_{(Y|X)} = 0.43 \pm 0.06$ dex. We call this tight correlation an *early-type sequence*. The $M_{\mathrm{BH}} - M_{*,\mathrm{sph}}$ log-relation for the bulges of late-type (spiral) galaxies has a slope of $2 - 3$, which is less well constrained due to the smaller size of the subsample and, more importantly, the smaller range in spheroid stellar mass ($3 \times 10^9 \lesssim M_{*,\mathrm{sph}}/\mathrm{M}_\odot \lesssim 3 \times 10^{10}$) that the subsample spans. We refer to this correlation as a "tentative" *late-type sequence*. In (gas-poor) early-type galaxies, the black hole

and the stellar content of the spheroidal component grow at the same pace, following a linear $M_{\rm BH} - M_{\rm *,sph}$ relation. In (gas-rich) spiral galaxies, the black hole grows faster than its host bulge, following a quadratic/cubic $M_{\rm BH} - M_{\rm *,sph}$ relation. For analogy with the color-magnitude diagram, it may be tempting to refer to our *early-type sequence* as a *red sequence* and to our *late-type sequence* as a *blue sequence*. Future work will explore the color of spheroids and galaxies in the $M_{\rm BH} - M_{\rm *,sph}$ diagram.

- The $M_{\rm BH} - M_{\rm *,sph}$ log-relations for core-Sérsic and Sérsic spheroids have slopes consistent with each other (1.19 ± 0.23 and 1.48 ± 0.20, respectively), thus these two populations do not appear to define two distinct sequences.

- In the $M_{\rm BH} - L_{\rm sph}$ (or $M_{\rm BH} - M_{\rm *,sph}$) diagram, for early-type galaxies, we did not observe the change in slope required for consistency with the log-linear $M_{\rm BH} - \sigma$ and bent $L_{\rm sph} - \sigma$ correlations. This issue of inconsistency remains therefore an open question. It might be that we are still not probing enough low-mass black holes ($M_{\rm BH} < 10^7 \, {\rm M_\odot}$) for the subsample of early-type galaxies, or that the transition from $L_{\rm sph} \propto \sigma^2$ at low luminosities to $L_{\rm sph} \propto \sigma^{(5-6)}$ at high luminosities is less sharp than previously thought. We intend to investigate this point in our future work.

- Spheroids with Sérsic index $n_{\rm sph} < 2$, argued by some to be pseudo-bulges, are not offset to lower $M_{\rm BH}$ from the $M_{\rm BH} - L_{\rm sph}$ correlation defined by spheroids with $n_{\rm sph} > 2$.

- The $M_{\rm BH} - L_{\rm gal}$ and $M_{\rm BH} - L_{\rm sph}$ correlations have the same level of intrinsic scatter when considering early-type galaxies only. Once reasonable numbers of spiral galaxies are included, $M_{\rm BH}$ correlates better with $L_{\rm sph}$ than with $L_{\rm gal}$.

REFERENCES

Akritas, M. G., & Bershady, M. A. 1996, ApJ, 470, 706

Arnold, J. A., Romanowsky, A. J., Brodie, J. P., et al. 2014, ApJ, 791, 80

Athanassoula, E. 2005, MNRAS, 358, 1477

Balcells, M., Graham, A. W., & Peletier, R. F. 2007, ApJ, 665, 1104

Bardeen, J. M. 1975, in IAU Symposium, Vol. 69, Dynamics of the Solar Systems, ed. A. Hayli, 297

Beifiori, A., Courteau, S., Corsini, E. M., & Zhu, Y. 2012, MNRAS, 419, 2497

Bekki, K. 2010, MNRAS, 401, L58

Bender, R. 1990, A&A, 229, 441

Capaccioli, M. 1987, in IAU Symposium, Vol. 127, Structure and Dynamics of Elliptical Galaxies, ed. P. T. de Zeeuw, 47–60

Cappellari, M., Emsellem, E., Krajnović, D., et al. 2011, MNRAS, 413, 813

Carter, D. 1987, ApJ, 312, 514

Chilingarian, I. V., Cayatte, V., Durret, F., et al. 2008, A&A, 486, 85

Cody, A. M., Carter, D., Bridges, T. J., Mobasher, B., & Poggianti, B. M. 2009, MNRAS, 396, 1647

Combes, F., Debbasch, F., Friedli, D., & Pfenniger, D. 1990, A&A, 233, 82

Combes, F., & Sanders, R. H. 1981, A&A, 96, 164

Davies, J. I., Phillipps, S., Cawson, M. G. M., Disney, M. J., & Kibblewhite, E. J. 1988, MNRAS, 232, 239

Davies, R. L., Efstathiou, G., Fall, S. M., Illingworth, G., & Schechter, P. L. 1983, ApJ, 266, 41

de Rijcke, S., Michielsen, D., Dejonghe, H., Zeilinger, W. W., & Hau, G. K. T. 2005, A&A, 438, 491

dos Anjos, S., & da Silva, M. B. 2013, Memorie della Societa Astronomica Italiana Supplementi, 25, 33

Dressler, A. 1989, in IAU Symposium, Vol. 134, Active Galactic Nuclei, ed. D. E. Osterbrock & J. S. Miller, 217

Eliche-Moral, M. C., González-García, A. C., Balcells, M., et al. 2011, A&A, 533, A104

Emsellem, , & E. et al. 2011, MNRAS, 414, 888

Erwin, P., Beltrán, J. C. V., Graham, A. W., & Beckman, J. E. 2003, ApJ, 597, 929

Erwin, P., & Gadotti, D. A. 2012, Advances in Astronomy, 2012, 4

Erwin, P., Saglia, R., Thomas, J., et al. 2015, in IAU Symposium, Vol. 309, IAU Symposium, ed. B. L. Ziegler, F. Combes, H. Dannerbauer, & M. Verdugo, 359–360

Fazio, G. G., Hora, J. L., Allen, L. E., et al. 2004, ApJS, 154, 10

Ferrarese, L., & Ford, H. 2005, Space Sci. Rev., 116, 523

Ferrarese, L., & Merritt, D. 2000, ApJ, 539, L9

Forbes, D. A., Lasky, P., Graham, A. W., & Spitler, L. 2008, MNRAS, 389, 1924

Gadotti, D. A. 2009, MNRAS, 393, 1531

Gavazzi, G., Boselli, A., Donati, A., Franzetti, P., & Scodeggio, M. 2003, A&A, 400, 451

Gebhardt, K., Bender, R., Bower, G., et al. 2000, ApJ, 539, L13

Graham, A. 2015a, Highlights of Astronomy, 16, 360

Graham, A. W. 2007, MNRAS, 379, 711

—. 2012, ApJ, 746, 113

—. 2013, Elliptical and Disk Galaxy Structure and Modern Scaling Laws, ed. T. D. Oswalt & W. C. Keel, 91

Graham, A. W. 2014, in Astronomical Society of the Pacific Conference Series, Vol. 480, Structure and Dynamics of Disk Galaxies, ed. M. S. Seigar & P. Treuthardt, 185

—. 2015b, ArXiv e-prints, arXiv:1501.02937

—. 2015c, ArXiv e-prints, arXiv:1501.02937

Graham, A. W., Erwin, P., Trujillo, I., & Asensio Ramos, A. 2003, AJ, 125, 2951

Graham, A. W., Onken, C. A., Athanassoula, E., & Combes, F. 2011, MNRAS, 412, 2211

Graham, A. W., & Scott, N. 2013, ApJ, 764, 151

—. 2015, ApJ, 798, 54

Graham, A. W., & Worley, C. C. 2008, MNRAS, 388, 1708

Gültekin, K., Richstone, D. O., Gebhardt, K., et al. 2009, ApJ, 698, 198

Häring, N., & Rix, H.-W. 2004, ApJ, 604, L89

TABLE 4
LINEAR REGRESSION ANALYSIS OF THE $M_{\rm BH} - M_{*,\rm sph}$ DIAGRAM.

Subsample (size)	Regression	α	β	$\langle M_{*,\rm sph} \rangle$	ϵ	Δ
	$\log[M_{\rm BH}/{\rm M}_\odot] = \alpha + \beta \log[(M_{*,\rm sph} - \langle M_{*,\rm sph} \rangle)/{\rm M}_\odot]$					
Core-Sérsic (22)	BCES $(Y\|X)$	9.06 ± 0.09	0.86 ± 0.28	11.28	–	0.42
	BCES $(X\|Y)$	9.06 ± 0.12	1.70 ± 0.32	11.28	–	0.61
	BCES Bisector	9.06 ± 0.10	1.19 ± 0.23	11.28	–	0.47
	FITEXY $(Y\|X)$	$9.06^{+0.08}_{-0.08}$	$0.68^{+0.21}_{-0.20}$	11.28	$0.36^{+0.09}_{-0.06}$	0.42
	FITEXY $(X\|Y)$	$9.03^{+0.15}_{-0.16}$	$1.90^{+0.85}_{-0.46}$	11.28	$0.62^{+0.13}_{-0.10}$	0.68
	FITEXY Bisector	$9.05^{+0.12}_{-0.13}$	$1.12^{+0.35}_{-0.27}$	11.28	–	0.46
	linmix_err $(Y\|X)$	9.04 ± 0.10	0.64 ± 0.25	11.28	0.40 ± 0.09	0.42
	linmix_err $(X\|Y)$	9.03 ± 0.17	1.80 ± 0.70	11.28	0.67 ± 0.30	0.65
	linmix_err Bisector	9.04 ± 0.14	1.06 ± 0.35	11.28	–	0.45
Sérsic (44)	BCES $(Y\|X)$	7.71 ± 0.09	0.95 ± 0.21	10.25	–	0.64
	BCES $(X\|Y)$	7.71 ± 0.16	2.52 ± 0.54	10.25	–	1.11
	BCES Bisector	7.71 ± 0.11	1.48 ± 0.20	10.25	–	0.74
	FITEXY $(Y\|X)$	$7.72^{+0.10}_{-0.09}$	$0.96^{+0.21}_{-0.21}$	10.25	$0.58^{+0.09}_{-0.07}$	0.64
	FITEXY $(X\|Y)$	$7.72^{+0.16}_{-0.16}$	$2.49^{+0.69}_{-0.45}$	10.25	$0.93^{+0.15}_{-0.13}$	1.10
	FITEXY Bisector	$7.72^{+0.13}_{-0.13}$	$1.49^{+0.33}_{-0.28}$	10.25	–	0.74
	linmix_err $(Y\|X)$	7.73 ± 0.10	0.98 ± 0.24	10.25	0.59 ± 0.08	0.65
	linmix_err $(X\|Y)$	7.73 ± 0.17	2.48 ± 0.59	10.25	0.95 ± 0.27	1.10
	linmix_err Bisector	7.73 ± 0.14	1.49 ± 0.57	10.25	–	0.74
Early-type (E+S0) (45)	BCES $(Y\|X)$	8.56 ± 0.07	0.85 ± 0.12	10.81	–	0.48
	BCES $(X\|Y)$	8.56 ± 0.09	1.27 ± 0.13	10.81	–	0.59
	BCES Bisector	$\mathbf{8.56 \pm 0.07}$	$\mathbf{1.04 \pm 0.10}$	**10.81**	–	**0.51**
	mFITEXY $(Y\|X)$	$8.56^{+0.06}_{-0.07}$	$0.83^{+0.11}_{-0.11}$	10.81	$0.42^{+0.07}_{-0.05}$	0.48
	mFITEXY $(X\|Y)$	$8.54^{+0.08}_{-0.09}$	$1.32^{+0.18}_{-0.15}$	10.81	$0.53^{+0.08}_{-0.07}$	0.61
	mFITEXY Bisector	$8.55^{+0.07}_{-0.08}$	$1.05^{+0.14}_{-0.12}$	10.81	–	0.51
	linmix_err $(Y\|X)$	8.55 ± 0.07	0.82 ± 0.12	10.81	0.43 ± 0.06	0.48
	linmix_err $(X\|Y)$	8.55 ± 0.09	1.29 ± 0.17	10.81	0.54 ± 0.11	0.59
	linmix_err Bisector	8.55 ± 0.08	1.03 ± 0.19	10.81	–	0.51
Late-type (Sp) (17)	BCES $(Y\|X)$	7.18 ± 0.17	1.95 ± 1.52	10.05	–	0.74
	BCES $(X\|Y)$	7.18 ± 0.39	5.89 ± 3.40	10.05	–	1.70
	BCES Bisector	$\mathbf{7.18 \pm 0.21}$	$\mathbf{3.00 \pm 1.30}$	**10.05**	–	**0.94**
	mFITEXY $(Y\|X)$	$7.20^{+0.15}_{-0.16}$	$1.22^{+0.70}_{-0.62}$	10.05	$0.59^{+0.16}_{-0.11}$	0.66
	mFITEXY $(X\|Y)$	$7.44^{+1.45}_{-0.52}$	$7.14^{+26.31}_{-3.01}$	10.05	$1.49^{+0.56}_{-0.36}$	2.08
	mFITEXY Bisector	$\mathbf{7.24^{+1.04}_{-0.39}}$	$\mathbf{2.28^{+1.67}_{-1.01}}$	**10.05**	–	**0.79**
	linmix_err $(Y\|X)$	7.23 ± 0.19	0.96 ± 0.96	10.05	0.67 ± 0.16	0.65
	linmix_err $(X\|Y)$	7.42 ± 0.64	6.96 ± 6.73	10.05	1.83 ± 1.86	2.03
	linmix_err Bisector	7.26 ± 0.47	1.94 ± 216.38	10.05	–	0.74

NOTE. — For each subsample, we indicate $\langle M_{*,\rm sph} \rangle$, its average value of spheroid stellar masses. In the last two columns, we report ϵ, the intrinsic scatter, and Δ, the total rms scatter in the $\log(M_{\rm BH})$ direction.

Held, E. V., de Zeeuw, T., Mould, J., & Picard, A. 1992, in IAU Symposium, Vol. 149, The Stellar Populations of Galaxies, ed. B. Barbuy & A. Renzini, 429

Hohl, F. 1975, in IAU Symposium, Vol. 69, Dynamics of the Solar Systems, ed. A. Hayli, 349

Jerjen, H., Binggeli, B., & Freeman, K. C. 2000, AJ, 119, 593

Jiang, Y.-F., Greene, J. E., & Ho, L. C. 2011, ApJ, 737, L45

Kelly, B. C. 2007, ApJ, 665, 1489

Keselman, J. A., & Nusser, A. 2012, MNRAS, 424, 1232

Kormendy, J. 2015, ArXiv e-prints, arXiv:1504.03330

Kormendy, J., & Ho, L. C. 2013, ARA&A, 51, 511

Kormendy, J., & Richstone, D. 1995, ARA&A, 33, 581

Kourkchi, E., Khosroshahi, H. G., Carter, D., et al. 2012, MNRAS, 420, 2819

Laor, A. 1998, ApJ, 505, L83

—. 2001, ApJ, 553, 677

Läsker, R., Ferrarese, L., & van de Ven, G. 2014a, ApJ, 780, 69

Läsker, R., Ferrarese, L., van de Ven, G., & Shankar, F. 2014b, ApJ, 780, 70

Lauer, T. R., Faber, S. M., Richstone, D., et al. 2007a, ApJ, 662, 808

—. 2007b, ApJ, 662, 808

Liu, F. S., Xia, X. Y., Mao, S., Wu, H., & Deng, Z. G. 2008, MNRAS, 385, 23

MacArthur, L. A., González, J. J., & Courteau, S. 2009, MNRAS, 395, 28

Magorrian, J., Tremaine, S., Richstone, D., et al. 1998, AJ, 115, 2285

Malumuth, E. M., & Kirshner, R. P. 1981, ApJ, 251, 508

Marconi, A., & Hunt, L. K. 2003, ApJ, 589, L21

Matković, A., & Guzmán, R. 2005, MNRAS, 362, 289

McConnell, N. J., & Ma, C.-P. 2013, ApJ, 764, 184

McConnell, N. J., Ma, C.-P., Gebhardt, K., et al. 2011, Nature, 480, 215

Meidt, S. E., Schinnerer, E., van de Ven, G., et al. 2014, ApJ, 788, 144

Montero-Dorta, A. D., Shu, Y., Bolton, A. S., Brownstein, J. R., & Weiner, B. J. 2015, ArXiv e-prints, arXiv:1505.03866

Nemmen, R. S., Georganopoulos, M., Guiriec, S., et al. 2012, Science, 338, 1445

Nieto, J.-L., Bender, R., Arnaud, J., & Surma, P. 1991, A&A, 244, L25

Peletier, R. F., Kutdemir, E., van der Wolk, G., et al. 2012, MNRAS, 419, 2031

Pfenniger, D., & Friedli, D. 1991, A&A, 252, 75

Press, W. H., Teukolsky, S. A., Vetterling, W. T., & Flannery, B. P. 1992, Numerical recipes in FORTRAN. The art of scientific computing

Querejeta, M., Eliche-Moral, M. C., Tapia, T., et al. 2015, A&A, 573, A78

Rix, H.-W., & White, S. D. M. 1990, ApJ, 362, 52

—. 1992, MNRAS, 254, 389

Rusli, S. P., Thomas, J., Saglia, R. P., et al. 2013, AJ, 146, 45

Ryan, C. J., De Robertis, M. M., Virani, S., Laor, A., & Dawson, P. C. 2007, ApJ, 654, 799

Saha, K., Martinez-Valpuesta, I., & Gerhard, O. 2012, MNRAS, 421, 333

Sani, E., Marconi, A., Hunt, L. K., & Risaliti, G. 2011, MNRAS, 413, 1479

Savorgnan, G. A. D., & Graham, A. W. 2015, MNRAS, 446, 2330

Scannapieco, C., White, S. D. M., Springel, V., & Tissera, P. B. 2011, MNRAS, 417, 154

Schechter, P. L. 1980, AJ, 85, 801

Scorza, C., & Bender, R. 1990, A&A, 235, 49

—. 1995, A&A, 293, 20

Scott, N., Davies, R. L., Houghton, R. C. W., et al. 2014, MNRAS, 441, 274

Scott, N., Graham, A. W., & Schombert, J. 2013, ApJ, 768, 76

Seidel, M. K., Cacho, R., Ruiz-Lara, T., et al. 2015, MNRAS, 446, 2837

Sheth, K., Regan, M., Hinz, J. L., et al. 2010, PASP, 122, 1397

Tortora, C., Napolitano, N. R., Romanowsky, A. J., Capaccioli, M., & Covone, G. 2009, MNRAS, 396, 1132

Tremaine, S., Gebhardt, K., Bender, R., et al. 2002, ApJ, 574, 740

Trujillo, I., Erwin, P., Asensio Ramos, A., & Graham, A. W. 2004, AJ, 127, 1917

van den Bosch, R. C. E., Gebhardt, K., Gültekin, K., et al. 2012, Nature, 491, 729

Vika, M., Driver, S. P., Cameron, E., Kelvin, L., & Robotham, A. 2012, MNRAS, 419, 2264

von der Linden, A., Best, P. N., Kauffmann, G., & White, S. D. M. 2007, MNRAS, 379, 867

Wandel, A. 1999, ApJ, 519, L39

Yee, H. K. C. 1992, in Astronomical Society of the Pacific Conference Series, Vol. 31, Relationships Between Active Galactic Nuclei and Starburst Galaxies, ed. A. V. Filippenko, 417

Young, C. K., & Currie, M. J. 1994, MNRAS, 268, L11